Modulated magnetic structure of Fe_3PO_7 as seen by ^{57}Fe Mössbauer spectroscopy

A. V. Sobolev, A. A. Akulenko, I. S. Glazkova, D. A. Pankratov, and I. A. Presniakov
M.V. Lomonosov Moscow State University, Chemistry Department, Moscow 119991, Russia

(Received 24 October 2017; published 22 March 2018)

The paper reports results of the ^{57}Fe Mössbauer measurements on an $Fe_3PO_4O_3$ powder sample recorded at various temperatures, including the point of magnetic phase transition $T_N \approx 163$ K. The spectra measured above T_N consist of a quadrupole doublet with high quadrupole splitting of $\Delta_{300\,K} \approx 1.10$ mm/s, emphasizing that Fe^{3+} ions are located in crystal positions with a strong electric-field gradient (EFG). To predict the sign and orientation of the main components of the EFG tensor, we calculated the EFG using the density-functional-theory approach. In the temperature range $T < T_N$, the experimental spectra were fitted assuming that the electric hyperfine interactions are modulated when the Fe^{3+} spin ($\boldsymbol{S}$) rotates with respect to the EFG axis, and with the emergence of spatial anisotropy of the hyperfine field $H_{hf} \propto \tilde{\boldsymbol{A}} \cdot \boldsymbol{S}$ at ^{57}Fe nuclei. These data were analyzed to estimate the components of the anisotropic hyperfine coupling tensor ($\tilde{\boldsymbol{A}}$). The large anharmonicity parameter, $m \approx 0.94$, of the spiral spin structure results from easy-axis anisotropy in the plane of the iron spin rotation. The temperature evolution of the hyperfine field $H_{hf}(T)$ was described by the Bean-Rodbell model, which takes into account that the exchange magnetic interactions are a strong function of the lattice spacing. The obtained Mössbauer data are in qualitative agreement with previous neutron-diffraction data for a modulated helical magnetic structure in strongly frustrated $Fe_3PO_4O_3$.

DOI: 10.1103/PhysRevB.97.104415

I. INTRODUCTION

The $Fe_3PO_4O_3$ (or Fe_3PO_7) phosphate, known in the literature as the mineral grattarolaite [1], forms a noncentrosymmetric crystal lattice consisting of triangular units $(Fe^{3+})_3$, which are coplanar with the hexagonal (ab) planes. The local coordination of Fe^{3+} ions is a distorted trigonal bipyramid (FeO_5) cluster. These clusters are arranged in triangular subunits linked to one face within the iron triangle. Below $T_N = 163$ K, previous magnetic and thermodynamic measurements [2] revealed very strong magnetic Fe^{3+} coupling ($\Theta_{CW} \sim -1000$ K) with frustration parameter, $|\Theta_{CW}|/T_N > 6$, indicating significant frustration of the antiferromagnetic interactions. According to the recent powder neutron-diffraction data [2], the strong frustration induces an ordered helical incommensurate structure with the helical axis in the hexagonal (ab) plane and a modulation wave vector of modulus $|\delta| = 0.073$ Å^{-1}. It was shown that the wave vector $\boldsymbol{k}_h = (\delta_a, \delta_b, 1.5)$ for the modulation does not change as a function of temperature. There are two types of near-neighbor magnetic exchange interactions (Fig. 1): the nearest-neighbor J_1 exchange ($z_1 = 2$) within the triangle $(Fe)_3$, and the J_2 exchange ($z_2 = 4$) coupling trigonal units in different c-axis layers. According to [2], the observed commensurate antiferromagnetic order along the c axis implies that the J_2 exchange is dominant, and the helical modulation within the (ab) plane arises as a compromise for the competing J_1-J_2 interactions.

One of the intriguing features of the magnetic structure in $Fe_3PO_4O_3$ is the needlelike domains [2]. The small in-plane correlation length (∼70 Å) persisting down to the lowest temperatures ($T \ll T_N$) blocks of long-range order of the helical magnetic structure. It was assumed that the appearance of domain walls in the structure is a result of the frustrated J_1 interactions within triangular $(Fe)_3$ units [2]. However, the mechanism for stabilization of domains in the antiferromagnetic phase is not well understood. Moreover, because of the high concentration of disordered domains, neutron diffraction on the powder does not allow us to determine uniquely the orientation of the helix axis within the (ab) plane.

In this work, we present the results of a detailed Mössbauer study of $Fe_3PO_4O_3$ in a wide temperature range, including magnetic phase transitions. Since previous ^{57}Fe Mössbauer data were reported only above T_N [3,4], we performed measurements down to 15 K in order to complement the study of the unusual magnetic structure of this triangle-based material. In the range $T < T_N$, the spectra are analyzed assuming a space-modulated helical magnetic structure proposed in [2]. Such an approach allows us to reproduce, from experimental spectra, the profile of the spatial anisotropy of the hyperfine field, H_{hf}, and the large easy-axis anisotropy in the plane of the iron spin rotation. We carried out a detailed analysis of the temperature dependences of hyperfine parameters in light of the peculiarities of the electronic and magnetic states of the iron ions in $Fe_3PO_4O_3$.

II. EXPERIMENT

The powder $Fe_3PO_4O_3$ sample was prepared by a two-step solid-state reaction. First, we prepared iron phosphate $FePO_4$ by mixing the stoichiometric amounts of $FeC_2O_4 \cdot 2H_2O$ and $NH_4H_2PO_4$, and then two-step annealing was performed at 350 °C for 12 h and at 620 °C for 12 h in air. Second, we mixed stoichiometric amounts of Fe_2O_3 and $FePO_4$ powders and annealed at 950 °C for 12 h, and finally we annealed several times at 1075 °C for 12 h.

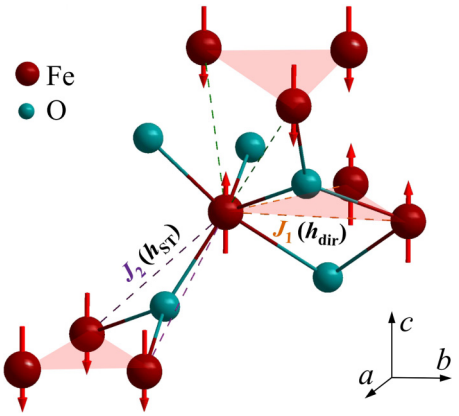

FIG. 1. Schematic of the magnetic surrounding of Fe^{3+} in Fe_3PO_7 [exchange interactions and integrals within (J_1) and between (J_2) the triangles $(Fe)_3$ along the c axis are shown]. Schematic representation of different contributions (h_{ST} and h_{dir}) to the H_{hf} value for the phosphate.

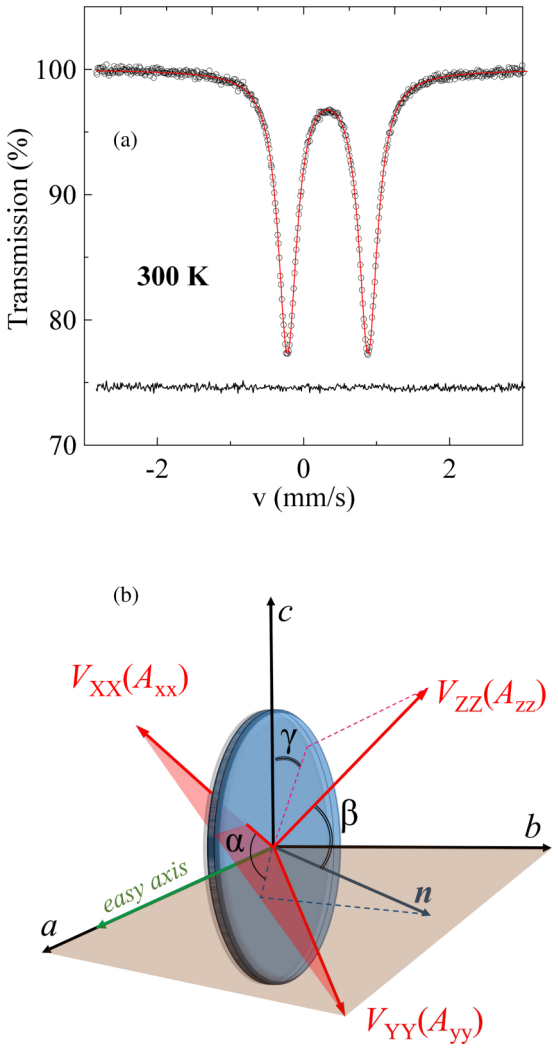

FIG. 2. (a) ^{57}Fe Mössbauer spectrum of Fe_3PO_7 recorded at $T = 298$ K ($T \gg T_N$) (the solid red line is the result of a simulation of the experimental spectra). (b) Schematic view of the local crystal structure of Fe_3PO_7 (in hexagonal base) and directions of the principal EFG $\{V_{ii}\}_{i=x,y,z}$ axes [$\{\alpha,\beta,\gamma\}$ are the Euler angles, describing the relation between the principal (XYZ) axes of the EFG tensor and the rotation plane].

X-ray powder diffraction (XRPD) data were collected at room temperature (RT) on a RIGAKU MiniFlex600 diffractometer using Cu $K\alpha$ radiation (a 2θ range of $10°-80°$, a step width of $0.02°$, and a scan speed of 1 deg/min). The XRPD patterns of the synthesized samples showed the formation of the unique rhombohedral $Fe_3PO_4O_3$ phase (space group $R3m$). The refined lattice parameters of $Fe_3PO_4O_3$ in hexagonal reference [$a = 8.006(1)$ Å and $c = 6.863(4)$ Å] are in good agreement with the literature data [3]. In what follows, the rhombohedral $Fe_3PO_4O_3$ phase will be referred to as "Fe_3PO_7".

Mössbauer experiments were performed in transmission geometry with a 1500 MBq γ-source of $^{57}Co(Rh)$ mounted on a conventional constant acceleration drive. The spectra were fitted using the SPECTRRELAX program [5]. The isomer shift values are reffered to that of α-Fe at 300 K.

Density-functional-theory (DFT) calculations [6] of quadrupole splitting were used to study the electronic state and crystal environment of iron in Fe_3PO_7. DFT calculations were made using the ORCA program [7]. The electric-field gradient was calculated for the cluster, which contains 40 atoms using the density B3LYP [8] functional available in the ORCA [7] package. The def2-TZVPP [9] basis for EFG tensor calculation was selected.

III. RESULTS AND DISCUSSIONS

The ^{57}Fe Mössbauer spectra of $Fe_3PO_4O_3$ measured in the paramagnetic temperature range ($T > T_N$) [Fig. 2(a)] consist of a single quadrupole doublet with narrow [$W = 0.31(1)$ mm/s] and symmetrical lines, emphasizing the uniformity of structural positions of iron atoms in the phosphate [3]. The value of the isomer shift $\delta_{300\,K} = 0.33(1)$ mm/s corresponds to high-spin ions Fe^{3+} (d^5, $S = 5/2$) located in oxygen (FeO_n) polyhedra with a coordination number $n > 4$ [10]. It is interesting that the observed δ value is closer to the typical values of isomer shifts ($\delta_{300\,K} \sim 0.36$ mm/s [10]) for Fe^{3+} ions in an octahedral oxygen surrounding where, in contrast to trigonal bipyramidal (FeO_5) polyhedra ($\delta_{300\,K} \sim 0.27$ mm/s [10]), the Fe-O bonds are considered to be almost entirely ionic. Apparently, this coincidence is due to the fact that the Fe ← O transfer of the electron density in trigonal bipyramidal (FeO_5) polyhedra induces a simultaneous increase in the $4s$ and $3d$ orbital populations of iron ions, which affects the value of the isomer shift in the opposite directions [10,11]. Mutual compensation of these two effects may render the resulting isomer shift "less sensitive" to specific chemical bonds of iron in oxides, in contrast to quadrupole splitting, which allows us to estimate the symmetry of the local surrounding and spin state of Fe^{3+} ions.

The high quadrupole splitting of the doublet $\Delta_{300\,K} = 1.10(1)$ mm/s shows that the ^{57}Fe nuclei are located in crystal positions with a strong electric-field gradient (EFG). As the EFG reflects the asphericity of the charge-density distribution near the probe ^{57}Fe nucleus, it is directly related to the electron-

density distribution and the symmetry in the nearest environment of the chemical bond. To get a better understanding of the charge redistribution effect in the Fe_3PO_7 lattice, we calculated the EFG using the DFT method [6]. The components (V_{ij}) of the EFG can be calculated directly from the electronic and nuclear charge distribution by [7]

$$V_{ij} = -\sum_{kl} P_{kl}\langle\phi_k|\left(\frac{3r_i r_j - \delta_{ij}r^2}{r^5}\right)|\phi_l\rangle + \sum_{k(t)} Z_t\left(\frac{3\xi_{ki}\xi_{kj} - \delta_{ij}R_k^2}{R_k^5}\right), \quad (1)$$

where r is the electronic position relative to the ^{57}Fe nucleus, R_k is the distance between ^{57}Fe and the nucleus "t," $r_{i(j)}$ and $\xi_{k,i(j)}$ $(i,j = x,y,z)$ are the projections of the vectors $\boldsymbol{r}$ and $\boldsymbol{R}_k$, respectively, $\phi_{k(l)}$ are the basis single-electron wave functions (e.g., "atomic" orbitals), and $\{P_{kl}\}$ are the elements of the density matrices [7]. The first contribution in (1) is the asymmetric distribution of the valence electrons ($\boldsymbol{V}^{\rm el}$) of the iron ion under consideration. The second is the lattice contribution ($\boldsymbol{V}^{\rm lat}$) arising from the point charges (Z_t) in the surroundings. The calculated $\boldsymbol{V}^{\rm el}$ and $\boldsymbol{V}^{\rm lat}$ values for the principal component V_{ZZ} (where $|V_{ZZ}| \geqslant |V_{YY}| \geqslant |V_{XX}|$) are $V_{ZZ}^{\rm el} = -9.40 \times 10^{21}$ V/m^2 and $V_{ZZ}^{\rm lat} = -3.05 \times 10^{21}$ V/m^2. Obviously, the total V_{ZZ} value is dominated by the valence electrons. To a good approximation, the valence contribution is determined by the anisotropy Δn_p and Δn_d of the p and d electrons [12]:

$$V_{ZZ}^{\rm el} = a\Delta n_p + b\Delta n_d = a\left(\tfrac{1}{2}\left[n_{p_x} + n_{p_y}\right] - n_{p_z}\right) + b\left(n_{d_{x2-y2}} + n_{d_{xy}} - \tfrac{1}{2}\left[n_{d_{xz}} + n_{d_{yz}}\right] - n_{d_{z2}}\right), \quad (2)$$

where $a \propto \langle r^{-3}\rangle_p$ and $b \propto \langle r^{-3}\rangle_d$ are the average values of the inverse radial functions of the p and d electrons. Using the Mulliken population analysis [13], we calculated the corresponding deviations $\Delta n_p = 0.018$ and $\Delta n_d = -0.035$ (see Table S1 of the Supplemental Material [27]). According to this evaluation, the anisotropy Δn_d is much more pronounced than that of Δn_p, indicating a stronger anisotropic spatial distribution of d electrons compared with that of the p electrons. The negative $V_{ZZ,3d}^{\rm el} \propto \Delta n_d$ value shows that excess charges are accumulated in the z direction, and the contributions from d_{xz}, d_{yz}, and d_{z2} orbitals dominate over those of d_{x2-y2} and d_{xy} orbitals oriented within the xy plane. Such a redistribution of d electrons agrees qualitatively with the local symmetry of the distorted trigonal bipyramid (FeO_5) clusters, where the apical Fe-O bonds are more elongated than the equatorial ones. It should be noted that although Δn_d is significantly greater than Δn_p, the much larger expectation value $\langle 1/r^3\rangle_{np}$ of the np radial functions causes the large contributions of the core np electrons (n = 1–3) to the EFG.

Using the calculated EFG components $V_{XX} = 2.154 \times 10^{21}$ V/m^2, $V_{YY} = 4.638 \times 10^{21}$ V/m^2, $V_{ZZ} = -6.792 \times 10^{21}$ V/m^2, and the asymmetry parameter $\eta = 0.366$ defined as the ratio $(V_{XX}-V_{YY})/V_{ZZ}$, we evaluated the quadrupole splitting $\Delta = eQV_{ZZ}/2(1+\eta^2/3)^{1/2}$ (taking the value of $Q = +0.16b$ for the nuclear quadrupole moment of ^{57}Fe [11]). A reasonable agreement between the experimental (1.01 mm/s) and theoretical (1.159 mm/s) values of Δ was obtained. The component V_{ZZ} was found to be negative as well, indicating that the quadrupole coupling constant eQV_{ZZ} is negative (for the positive Q). The calculations revealed that the V_{ZZ} component makes an angle of $\beta \approx 40^\circ$ with the c axis in a hexagonal coordinate system [Fig. 2(b)] and a positive V_{YY} component perpendicular to the c axis, thus V_{YY} is lying in the plane (ab) at about 60° from the b axis.

Below $T_{\rm N} \approx 163$ K, a complex Zeeman magnetic structure appears in the Mössbauer spectra (Fig. 3). The observed inhomogeneous line broadenings of the spectra reflect a high degree of correlation between the values of the magnetic hyperfine field $H_{\rm hf}$ at ^{57}Fe nuclei and a quadrupole shift (ε_Q) of the Zeeman components. It should be noted that a similar hyperfine magnetic structure was observed for the iron oxides $BiFeO_3$ [14,15], $AgFeO_2$ [16], and $FeVO_4$ [17] possessing a noncollinear magnetic structure. To describe the inhomogeneous line broadening, we took into account the dependence of the quadrupole shift ε_Q on the polar (θ) and azimuthal (ϕ) angles of the magnetic hyperfine field $\boldsymbol{H}_{\rm hf}$ with respect to the principal axes of the EFG tensor. The goodness of fit has been significantly improved using the first ($\varepsilon_Q^{(1)}$) and second ($\varepsilon_Q^{(2)}$) order of perturbation theory [18]:

$$\varepsilon_Q^{(1)} = (-1)^{|m_I|+1/2}\left(\tfrac{1}{8}eQV_{ZZ}\right)[3\cos^2\theta - 1 + \eta\sin^2\theta\cos 2\phi]$$

$$\varepsilon_Q^{(2)} = (-1)^{|m_I|+1/2}\frac{\left(\frac{1}{4\sqrt{2}}eQV_{ZZ}\right)^2}{g_{\rm ex}\mu_{\rm n}H_{\rm hf}}\left([6 - 4\eta\cos 2\phi]\cos^2\theta + \xi\left[\tfrac{3}{2}\sin^2\theta + \eta(1+\cos^2\theta)\cos 2\phi\right]\right)\sin^2\theta, \quad (3)$$

where m_I are magnetic quantum numbers; eQV_{ZZ} is the quadrupole splitting constant, which equals that in the paramagnetic state ($T > T_{\rm N}$) if there is no distortion of the crystal lattice at $T_{\rm N}$, $\xi = \pm 1/2$ is a coefficient depending on the specific line in the Zeeman structure, μ_n is the nuclear Bohr magneton, and $g_{\rm ex}$ is the gyromagnetic ratio of the excited state. In our model, we suggested also a spatial anisotropy of the hyperfine field $H_{\rm hf} \propto \tilde{\boldsymbol{A}} \cdot \boldsymbol{S}$ at the ^{57}Fe nuclei, which can be described as angular dependency of the hyperfine coupling tensor ($\tilde{\boldsymbol{A}}$) in the system defined by the principal axes of the EFG tensor [Fig. 2(b)]. For systems in which the anisotropy is not too large, in place of the actual field $\boldsymbol{H}_{\rm hf}$, we use the component $\tilde{\boldsymbol{A}} \cdot \boldsymbol{S}$ parallel to the spin direction $h_\parallel \equiv H_{\rm hf}(\parallel \boldsymbol{S})$. For the general case, $A_{xx} \neq A_{yy} \neq A_{zz}$, the expression for $h_\parallel$ is written in the following form:

$$h_{||}/S = \tilde{A}_{\rm is} + 1/6\tilde{A}_{\rm an}(3\cos^2\theta - 1) + \eta_m\sin^2\theta\cdot\cos 2\phi, \quad (4)$$

where $\tilde{A}_{is} = 1/3[A_{xx} + A_{yy} + A_{zz}]$ and $\tilde{A}_{\rm an} = [2A_{zz} - A_{xx} - A_{yy}]$ are isotropic and anisotropic parts of the hyperfine coupling tensor $\tilde{\boldsymbol{A}}$, respectively, and $\eta_m = 1/2[A_{xx} - A_{yy}]$ is the magnetic asymmetry parameter. Both angles θ and ϕ can be expressed by the angle ϑ, describing the position of the magnetic moment vector $\boldsymbol{\mu}_{\rm Fe}$ on the rotation plane, and the Euler angles ($\alpha\beta\gamma$), describing the relation between the principal (XYZ) axes of the EFG tensor and the rotation plane [Fig. 2(b)]. Therefore, the experimental spectrum is approximated as a superposition of the Zeeman patterns, and each of them is characterized by a different value of the rotation angle ϑ, which varies continuously in the $0 \leqslant \vartheta \leqslant 2\pi$ interval. The fitting was done using formulas

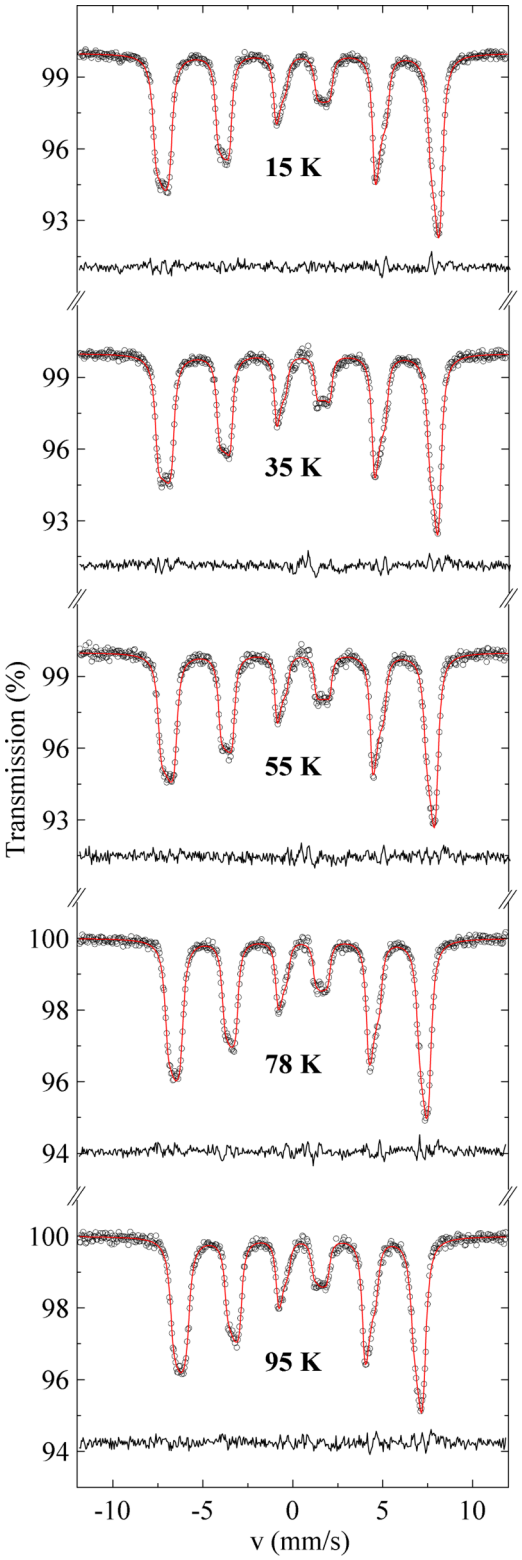

FIG. 3. ^{57}Fe Mössbauer spectra (experimental hollow dots) of Fe_3PO_7 recorded at the indicated temperatures below T_N. Solid red lines are a simulation of the experimental spectra as described in the text.

(1) and (2) in different iron sites. Finally, to take into account the anharmonicity (bunching) of the spatial distribution of the magnetic moments of Fe^{3+}, a Jacobian elliptic function

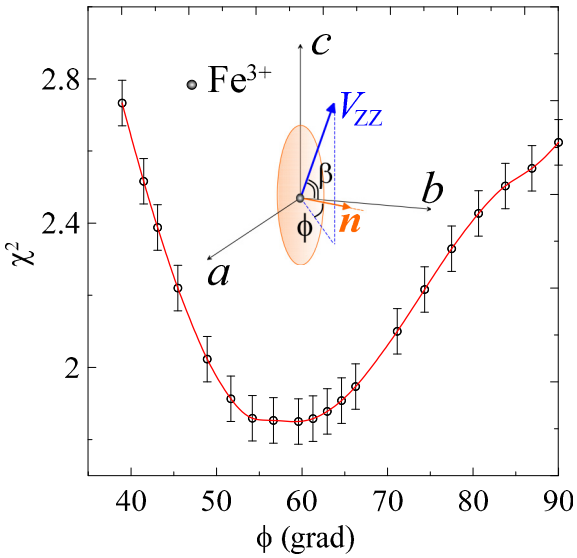

FIG. 4. The resulting χ^2 values for the fits of the spectra as a function of the variation in the angle (ϕ) between the helical plane direction $\boldsymbol{n}$ and the projection of the principal component V_{ZZ} on the (ab) plane (see the inset). The ϕ angle is directly related to Euler angle $\phi = \cos^{-1}\{\cos\beta/0.643\}$.

[16,19] was used:

$$\cos\vartheta(x) = \mathrm{sn}([\pm 4\ \mathrm{K}(m)/\lambda]x, m), \tag{5}$$

where λ is the period of the helicoid, $K(m)$ is the complete elliptic integral of the first kind, and m is the anharmonicity parameter related to the distortion (anharmonicity) of the spiral structure [16].

According to the helicoidal magnetic structure of Fe_3PO_7 [2], the magnetic moments $\boldsymbol{\mu}_{Fe}$ are constant in magnitude and rotate in the plane containing the hexagonal c axis. However, using only the neutron powder diffraction data, the determination of the helical plane direction ($\boldsymbol{n}$) in the (ab) plane is difficult due to domain and powder averaging [2]. Therefore, applying the above fitting procedure, we systematically investigated a range of the angle β ($50^\circ \leqslant \beta \leqslant 90^\circ$) by taking two other Euler angles (α,γ) as adjustable parameters. In additional to the usual variables (δ,eQV_{ZZ}), assumed to be equal for all Zeeman subspectra, the principal components $\{A_{xx}, A_{yy}, A_{zz}\}$ of the tensor $\tilde{\boldsymbol{A}}$ and the anharmonicity parameter m were used as adjustable parameters. The value of the asymmetry parameter $\eta = 0.366$ evaluated from the point-charge calculations was fixed during the fitting processes. The resulting χ^2 values for the fits are shown in Fig. 4 as a function of the variation in the angle ϕ between the helical plane direction $\boldsymbol{n}$ and the projection of the principal component V_{ZZ} on the (ab) plane (see the inset of Fig. 4). This angle is directly related to the Euler angle $\phi = \cos^{-1}\{\cos\beta/0.643\}$ in accordance with the directions of the EFG principal components calculated previously. It is clearly visible that the best fit is obtained when the helical plane direction $\boldsymbol{n}$ is oriented in the (ab) plane at $\phi = 55^\circ$–65° (or about 30° from the a axis). This fit to the 15 K spectrum, obtained in this way, is shown in Fig. 3. Then, we tentatively fitted the spectrum assuming that the $\boldsymbol{n}$ direction is perpendicular to the hexagonal (ab) plane that corresponds

to the Euler angle $\beta \approx 50^\circ$ [Fig. 2(b)]. However, in this case the fit was of much poorer quality ($\chi^2 \approx 5.64$) than previous ones, and this supposition should be ruled out. At this point we can note that the analysis of the complex Mössbauer spectra at $T \ll T_N$ not only confirms several features of the helicoidal magnetic structure proposed in [2], but it also allows us to refine the helical plane direction, which cannot be determined from neutron powder diffraction data.

The hyperfine parameters deduced from the spectrum at $T = 15$ K are $\delta = 0.43(1)$ mm/s, $eQV_{ZZ} = -2.28(2)$ mm/s, and $W = 0.32(1)$ mm/s. The fitted quadrupole coupling constant eQV_{ZZ} has the same order of magnitude as the double quadrupole splitting ($2\Delta_{170\,\mathrm{K}} \approx 2.23$ mm/s) measured just above $T_N \approx 160$ K. The inequality of the principal components $A_{xx}S = 458(1)$ kOe, $A_{yy}S = 465(1)$ kOe, and $A_{zz}S = 472.4(3)$ kOe reflect the spatial anisotropy of the hyperfine field. Using these values, we traced a polar diagram of the spatial anisotropy in the system defined by the principal axes of the rhombic ($\eta \neq 0$) EFG tensor [Fig. 5(a)]. The projections of the $\boldsymbol{H}_{\mathrm{hf}}$ vector on the helical plane generate an elliptical-like profile with the maximal $H_\alpha \approx 469.3(5)$ kOe and minimal $H_\beta \approx 472.1(5)$ kOe components [Fig. 5(b)]. The diagonal components (A_{ii}) of the hyperfine tensor $\tilde{\boldsymbol{A}}$ are composed of three contributions:

$$A_{ii} \approx P_{\mathrm{Fe}}\left[-\frac{4\pi}{3}\rho(0) + \frac{1}{2}\langle r^{-3}\rangle_d(g_{ii}-2) + \sum_{\mu\nu} P^{\sigma}_{\mu\nu}\langle\phi_\mu|\left(\frac{3r_i^2 - r^2}{r^5}\right)|\phi_\nu\rangle\right], \quad (6)$$

where $P_{\mathrm{Fe}} = g_e g_N \beta_e \beta_N$ is the proportionality factor, $\mathrm{P}^{\sigma}_{\mu\nu}$ is the spin-density matrix, r is a radius vector that points from the nucleus to the electron, $\rho(0)$ is the spin density at the iron nucleus, $\{g_{ii}\}_{i=x,y,z}$ are the components of the effective $\tilde{g}^{\mathrm{eff}}$ tensor, and $\{\phi_k, \phi_l, \ldots\}$ is the set of basis $3d$ functions. The first term in Eq. (6) is the isotropic Fermi contact contribution, which determines the sign of the hyperfine tensor.

The anisotropy arises from the second and third terms in Eq. (6) corresponding to the orbital ($\tilde{\boldsymbol{A}}^{\mathrm{orb}}$) and the electronic dipolar ($\tilde{\boldsymbol{A}}^{\mathrm{dip}}$) components, respectively. The orbital term $\tilde{\boldsymbol{A}}^{\mathrm{orb}}$ corresponds to the magnetic field produced at the nucleus due to orbital currents. In general, the low-symmetry crystal field quenches the orbital angular moment, but the spin-orbit coupling restores it to an amount of $L_i \propto (g_{ii} - 2)S$ [7]. Thus, the anisotropic orbital term arises from the anisotropy of the $\tilde{g}^{\mathrm{eff}}$ tensor, which differs very little from ~2 for the high-spin Fe^{3+} ions with an A_{1g} orbital singlet ground state. The dipolar term $\tilde{\boldsymbol{A}}^{\mathrm{dip}}$ does not vanish only when the spin density is aspherical. For isolated high-spin Fe^{3+} ions with a spherical $3d$ electron distribution, this term becomes zero. However, covalent effects due to the anion-cation Fe^{3+}-$O^{2-} \rightarrow Fe^{2+}$-$O^{-}(\underline{L})$ charge transfer in the low-symmetry distorted FeO_n polyhedra produce interconfigurational mixing effects, particularly mixing of the $(3d^5)^6A_{1g}$ term with the orbitally active $(d^6\underline{L})\ ^6T_{1g}/^6T_{2g}$ terms for the charge-transfer configuration $d^6\underline{L}$, where $\underline{L}$ denotes the oxygen hole. As a result, we arrive at nonzero $\tilde{\boldsymbol{A}}^{\mathrm{dip}}$. To verify this assumption, we

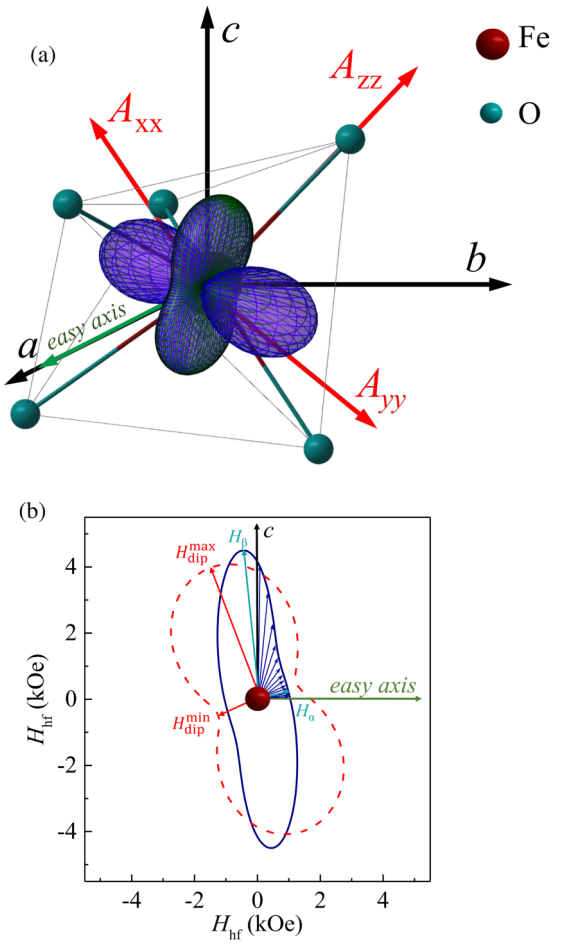

FIG. 5. (a) Surface plot of the $\tilde{\boldsymbol{A}}$ tensor relative to the principal EFG $\{V_{ii}\}_{i=x,y,z}$ axes, and (b) the ellipticlike contour of this function in the rotation plane of magnetic moments of iron ions. Distribution of $H_{\mathrm{hf}} \propto \tilde{\boldsymbol{A}} \cdot \boldsymbol{S}$ was calculated using formula (4) in 250 different iron sites (represented schematically by blue arrows) and taking the anharmonicity parameter $m \approx 0.94$ [H_α and H_β denote the maximal (H_α) and minimal (H_β) anisotropic hyperfine-field components]. The red dashed line corresponds to the projection of the dipolar field $h^D(\vartheta)$ [see Eq. (8)] on the spin rotation plane.

used the Mulliken populations ($n_{3d}^{\uparrow(\downarrow)}$) of the spin-polarized $3d$ orbitals (see Table S1 of the Supplemental Material [27]) obtained from the DFT calculations. Substituting these values into the expressions for the principal $A_{ii}^{\mathrm{dip}}[n_{3d}^{\uparrow(\downarrow)}]$ components [Eq. (S3) of the Supplemental Material], we evaluated the theoretical values $A_{xx}^{\mathrm{dip}}S = -0.53$ kOe, $A_{yy}^{\mathrm{dip}}S = -0.04$ kOe, and $A_{zz}^{\mathrm{dip}}S = 0.57$ kOe, the difference between which is significantly less than the corresponding experimental values. The above estimates show that the observed anisotropy of the hyperfine field in our experiments at the ^{57}Fe nuclei is not related to the intrinsic features of an iron electronic state in Fe_3PO_7 (nonquenched orbital contribution, reduced spin state, anisotropic charge-transfer, etc.) as was assumed previously in Ref. [2].

Another "external" source of an anisotropy of the local field $\boldsymbol{H}_{\mathrm{hf}}$ at the nucleus of the high-spin Fe^{3+} ions is a dipole field

$\tilde{\boldsymbol{A}}^{D}$ induced by the neighboring magnetic ions:

$$A_{ii}^{D} = \frac{\mu_0}{4\pi} \sum_{k(t)} \frac{\left(3\xi_{ik}^2 - R_k^2\right)}{R_k^5} \mu_{ik}, \tag{7}$$

where $k(t)$ is the summarized index on all positions of the t ion, $\xi_{ik} = \{x_k, y_k, z_k\}$ and R_k are Descartes coordinates (refer to the principal EFG axes frame) and the radius vector of the t ion in position $k(t)$, and μ_{ik} is the projection of the iron magnetic moment. Substituting in Eq. (4) the coordinates (ξ_{ik}) of the iron ions within the triangle plane and in different c-axis layers, taken from [2], the values of dipole contributions were evaluated: $A_{xx}^{D} = -2.1$ kOe, $A_{yy}^{D} = -4.6$ kOe, and $A_{zz}^{D} = 6.7$ kOe.

Using these values, we calculated the anisotropic part of the hyperfine coupling tensor $A_{\text{an}}^{D} = 20$ kOe associated with the dipole field, which is close to the experimental value of $\tilde{A}_{\text{an}} = 20.8(8)$ kOe from Eq. (4). We thus conclude that the main contribution to the observed spatial anisotropy of $\boldsymbol{H}_{\text{hf}}$ is due to the anisotropy of the dipole field $\tilde{\boldsymbol{A}}^{D}$ induced by the neighboring iron ions.

Since the large isotropic contribution to the internal $\boldsymbol{H}_{\text{hf}}$ field resulting from the Fermi contact interaction of the intrinsic spin of the Fe^{3+} ion with ns electrons exceeds by two orders of magnitude the anisotropic contribution, one may take into account only the projections of the anisotropic fields (h^{D}) on the direction of the isotropic hyperfine field:

$$h^{D}(\vartheta) = \frac{\mu_0}{4\pi} \sum_{k(t)} \mu_k \frac{\left(3x'^2_k - r_k^2\right)\cos^2\vartheta + \left(3y'^2_k - r_k^2\right)\sin^2\vartheta + x'_k y'_k \cos\vartheta \sin\vartheta}{R_k^5}, \tag{8}$$

where ϑ is between the direction of H_{hf} and the local x' axis oriented perpendicular to the hexagonal c axis, which is located within the $(x'y')$ plane of spin rotation [Fig. 5(b)], and μ_0 is the permeability constant. Using the above expression (in the coordinate system where the iron ion spin rotates), we plotted a polar diagram $h^{D}(\vartheta)$ [in Fig. 5(b)], which qualitatively reproduces the distorted ellipticlike profile of the experimental hyperfine field $\boldsymbol{H}_{\text{hf}}(\vartheta)$. Notice that the axes H_α and H_β of the ellipse do not necessarily coincide with the principal axes x' and y' of the $\tilde{\boldsymbol{A}}^{\text{dip}}$ tensor oriented in the $(x'y')$ plane at $\sim 20^\circ$ from the $c(\sim \parallel y')$ axis [Fig. 5(b)]. Some deviations of these profiles may be related with the small contribution of the anisotropic field $\sim(\tilde{\boldsymbol{A}}^{\text{orb}} + \tilde{\boldsymbol{A}}^{\text{dip}}) \cdot \boldsymbol{S}$ due to the reduction of the symmetry of the Fe^{3+} wave functions from cubic symmetry into low-symmetry crystal field.

The use of the above model allowed us to satisfactorily describe the entire series of experimental spectra measured in the magnetic ordering temperature range $15\,\text{K} \leqslant T < T_{\text{N}}$ (Fig. 3). We could not find any visible anomalies in the temperature dependences of hyperfine parameters (Fig. 6). The isomer shift $\delta(T)$ gradually decreases in accordance with the Debye approximation for the second-order Doppler shift [10] [Fig. 6(a)]. The best fit for the effective Debye temperature $\Theta_D = 552(3)$ K is in good agreement with the corresponding values for the Fe^{3+} ions in other iron oxides [11]. In the same temperature range, the observed $eQV_{ZZ}(T)$ dependence [inset of Fig. 6(a)] is mainly due to the temperature variation of the lattice $\boldsymbol{V}^{\text{lat}}(T)$ contribution to the EFG, which can be described using a semiempirical relation $|eQV_{ZZ}(T)| = A(1 - BT^{3/2})$ with $A = 2.277(9)$ mm/s and $B = 5.8(8) \times 10^{-6}\,\text{K}^{-3/2}$.

Taking into account the pronounced temperature dependence of the Fe_3PO_7 crystal parameters near T_{N} [2], the temperature dependence of the magnetic field $H_{\text{hf}}(T) = S/3\{A_{xx}(T) + A_{yy}(T) + A_{zz}(T)\}$ can be analyzed using the Bean-Rodbell (BR) model [20] rather than the normal Brillouin function [Fig. 6(b)]. In this approximation [20], the exchange magnetic interactions are considered to be a sufficiently strong function of the lattice spacing, and the hyperfine field $H_{\text{hf}}(T)$ is expressed as

$$H_{\text{hf}}(T) = H_{\text{hf}}(0) B_S\left[\frac{3S}{S+1}\frac{\sigma(T)}{\tau} \times \left(1 + \frac{3}{5}\frac{(2S+1)^4 - 1}{2(S+1)^3 S}\zeta\sigma^2(T)\right)\right], \tag{9}$$

where $S = 5/2$ is the total spin of the Fe^{3+} ions, $\sigma(T)$ is reduced hyperfine field $H_{\text{hf}}(T)/H_{\text{hf}}(0)$, $\tau = T/T_{\text{N}}$ is the reduced temperature, $H_{\text{hf}}(0)$ is the saturation hyperfine magnetic field, and ζ is the fitting parameter, which involves the magnetostructural coupling coefficient. The value of this parameter controls the order of the magnetic phase transition [20]. A reasonably good fit to the BR model was obtained for a magnitude of $\zeta = 0.53(1)$, which indicates a second-order phase transition. We estimated the saturation field $H_{\text{hf}}(0) = 461.5(4)$ kOe and the point $T_{\text{N}} \approx 168(1)$ K, which is close to the Néel point ($\sim$ 163 K) found from magnetic measurements [20]. This shows that there are no electronic and structural transitions in the whole magnetically ordered temperature range.

Alternatively, the temperature dependence of $H_{\text{hf}}(T)$ can be approximated using a power law $H_{\text{hf}}(T) = H_{\text{hf}}(0)[1\text{–}(T/T_{\text{N}})^{\alpha}]^{\beta}$, where β is a critical exponent and α is an empirical fitting parameter to describe the experimental data well below T_{N} ($T \ll T_{\text{N}}$). A reasonably good fit [Fig. 6(b)] leads to $H(0) = 473(2)$ kOe, $T_{\text{N}} = 165.4(8)$ K, $\alpha = 1.5(1)$, and $\beta = 0.24(1)$. The value of the critical exponent corresponds well to the theoretical value $\beta^{\text{th}} = 0.23$ expected for a system with two-dimensional (2D) XY magnets [21]. However, the origin of the critical parameter β in the quasi-2D systems is far from trivial due to the competition between several interactions, such as the magnetic coupling between layers and the strength of the crystal field (single-ion anisotropy), which can lead to a range of β values in the range $0.20 \leqslant \beta \leqslant 0.36$. Further experimental and theoretical study is still required to reach a deeper understanding of the critical dynamics and to give a more definitive assignment of the universality class of this very interesting system.

In the temperature range near T_{N} ($T \to T_{\text{N}}$), we observed the rapid broadening of the Zeeman lines and then the

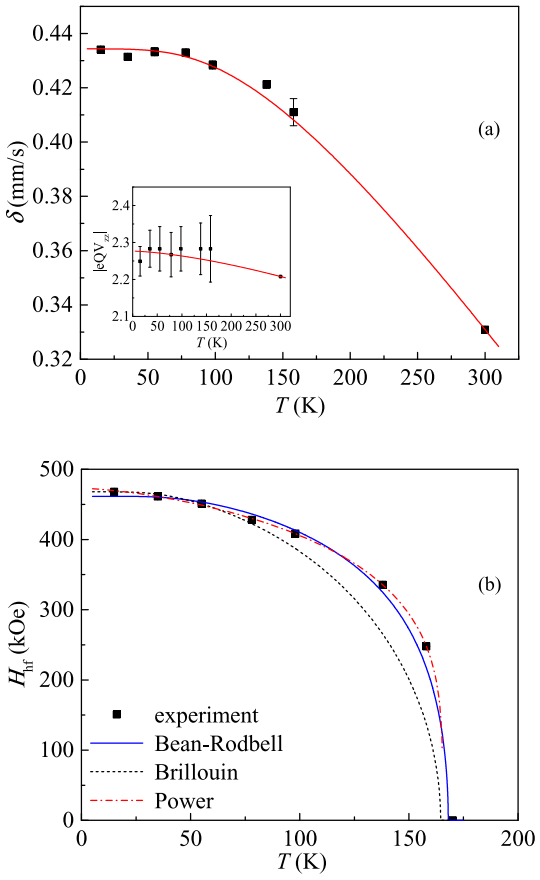

FIG. 6. (a) Isomer shift $\delta(T)$ as a function of the reduced temperature (the red solid line corresponds to the Debye approximation for the second-order Doppler shift), and quadrupole coupling constant eQV_{ZZ} (inset) plotted vs temperature (the red solid line corresponds to the fitting using the semiempirical relation; see the text). (b) Temperature dependence of hyperfine magnetic field $H_{\rm hf}(T)$. The dark broken line shows the Brillouin function with $S = 5/2$; the blue solid line corresponds to a fit using the Bean-Rodbell model; the dashed-dotted line indicates the power-law fit model.

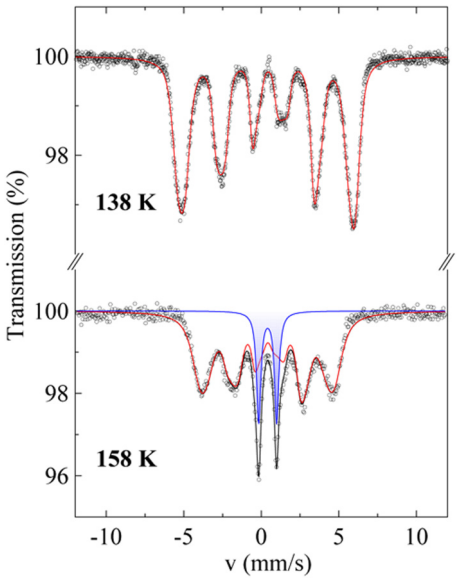

FIG. 7. ^{57}Fe Mössbauer spectra (experimental hollow dots) of Fe_3PO_7 recorded near the Néel temperature ($T \to T_{\rm N}$). Solid lines are a simulation of the experimental spectra as the superposition of magnetic (red line) and paramagnetic (blue line) subspectra.

appearance of a paramagnetic quadrupole doublet whose partial contribution increases sharply with temperature (Fig. 7). The hyperfine parameters (δ, Δ) of the doublet correspond well to those observed for the paramagnetic temperature range. Such a spectral behavior is characteristic of isolated superparamagnetic particles or nanosized magnetic domains with the randomly flipping direction of the magnetization under the influence of temperature. In the case of Fe_3PO_7, the needlelike domains can block the long-range magnetic order near the point $T_{\rm N}$, suggesting strong thermal spin fluctuations. It should be noted that the description of the experimental spectra was obtained by using anomalously high values of the anharmonicity parameter $m \approx 0.94(1)$, which remains almost constant in the range $T < T_{\rm N}$. We can speculate that the strong anisotropy is also associated with the presence of the needlelike domains. The best fit of the spectra is obtained when the easy (bunching) axis is directed along the line of intersection of the helical plane and the hexagonal (ab) plane [Fig. 2(b)]. It is possible that the domain walls create local stresses in the (ab) plane causing a nonuniform rotation of the iron spins.

Finally, we will comment on the lower value of the saturated magnetic field $H_{\rm hf}(0) \approx 462$ kOe of Fe_3PO_7 in comparison to the 540–568 kOe values for the high-spin ferric ions in other 3D oxide systems [22]. This reduction can be related to the local magnetic surrounding of Fe^{3+} ions via the transferred hyperfine field resulting from all the nearest ferric neighbors along the c axis and within the (ab) plane. The experimental hyperfine field $\boldsymbol{H}_{\rm hf}$ is the vector sum of two main contributions:

$$\boldsymbol{H}_{hf} = H_{\rm loc} + \sum_{\rm n} B_{\rm n}(\langle S_{\rm n}/S\rangle), \tag{10}$$

where $\boldsymbol{H}_{\rm loc} = \boldsymbol{H}_{\rm F} + \boldsymbol{H}_{\rm cov}$ is the local field that is the sum of the free-ion field $\boldsymbol{H}_{\rm F}$, produced by the Fermi contact interaction, and the covalent contribution $\boldsymbol{H}_{\rm cov}$, arising from the covalent transfer effects [23]. These two contributions are proportional to the vector $\langle \boldsymbol{S}\rangle$ directed along the thermally averaged $3d$ spins. According to theoretical calculations [24,25], $H_{\rm loc} \approx$ (490–500) kOe for Fe^{3+} ions in octahedral coordination, and $H_{\rm loc} \approx$ (410–420) kOe for Fe^{3+} ions located in a tetrahedral oxygen surrounding. Unfortunately, we do not have any information concerning Fe^{3+} in a trigonal bipyramid. The second term in (10) is a contribution resulting from all single-bridged nearest ferric neighbors "n," each proportional to the spin $\langle \boldsymbol{S}_n\rangle$ on the neighboring site, and B_n is a positive scalar parameter depending on the superexchange iron-oxygen-iron bond angle (ψ) and the direct iron-iron bond distance [23]:

$$B_{\rm n} = \left\{\left(h_\sigma^{(n)} - h_\pi^{(n)}\right)\cos^2\psi_n + h_\pi^{(n)}\right\}_{\rm ST} + h_{\rm dir}^{(n)}, \tag{11}$$

where h_σ and h_π parameters arise from the supertransferred (ST) spin-polarization of iron s orbitals, caused by the ligand p orbitals that have been unpaired by spin transfer, via σ and π bonds, into unoccupied $3d$ orbitals on the neighboring cations; $h_{\rm dir}$ is the direct contribution arising from the overlap distortions of iron s orbitals by $3d$ orbitals of the neighboring ions. The calculations of Moskvin *et al.* [25] for ferrites

$R\mathrm{FeO_3}$ have shown that $|h_\sigma| \approx 10$ kOe and $|h_\pi| \approx 1.6$ kOe. For the face-shared $\mathrm{FeO_5}$ pyramids, due to the compensation effect of the weakened antiferromagnetic kinetic exchange with the ferromagnetic potential *s-d* exchange [25], the direct contribution $|h_{\mathrm{dir}}|$ usually does not exceed 9–12 kOe [16].

$\mathrm{Fe_3PO_7}$ exhibits noncollinear magnetic order, in which among six iron neighbors of the central iron there are two nearest neighbors with the same spin direction as the central ion and coupled with this one through direct exchange interactions (Fig. 1). The remaining four neighbors from triangular units in different *c*-axis layers, connected with the central ion by the supertransferred interactions Fe-O-Fe, have the opposite spin direction. Substituting in Eq. (11) the values of the angle $\psi \approx 125^\circ$ [15] and parameters $h_\sigma = 10$ kOe and $h_\pi = 2$ kOe [25], we evaluated the positive supertransferred contribution $H_{\mathrm{ST}} = 4 \times B_{\mathrm{ST}} \approx 18$ kOe from Fe^{3+} ions in triangular units located in adjacent *c*-axis layers (a slight noncollinearity of neighboring iron moments leads to an error of not more than a few percent). This small positive contribution can be largely compensated by the negative "direct" contribution $H_{\mathrm{dir}} = -2 \times h_{\mathrm{dir}} \approx -(18\text{–}24)$ kOe from the two neighbors with the same spin directions as the central iron ion, giving a total contribution of zero to the H_{hf} field. As a result, the reduced H_{hf} value for $\mathrm{Fe_3PO_7}$ is presented as $H_{\mathrm{hf}} \approx H_{\mathrm{F}} + H_{\mathrm{cov}}$, where the large negative contribution $H_{\mathrm{cov}} = H_{\mathrm{hf}} - H_{\mathrm{F}} \approx -168$ kOe (we have chosen $H_{\mathrm{F}} = 630$ kOe [26]) arises from the Fe^{3+}-$O^{2-} \rightarrow Fe^{2+}$-$O^{-}(\underline{L})$ charge transfer (where $\underline{L}$ denotes the oxygen hole). This conclusion agrees with the previously proposed explanation for the reduced effective moment per Fe^{3+} ($\mu_{\mathrm{eff}} \sim 4.2\,\mu_B$) [2] in $\mathrm{Fe_3PO_7}$, attributed to the charge transfer in this insulating compound. Finally, the charge transfer $O^{2-} \rightarrow Fe^{3+}$ in the low-symmetry distorted $\mathrm{FeO_5}$ polyhedra produces interconfigurational mixing effects, particularly mixing of the ${}^6A_{1g}(d^5)$ term with the orbitally active ($\langle L \rangle \neq 0$) ${}^6T_{1g}(d^6\underline{L})$ term, inducing the single-ion anisotropy for the charge-transfer configuration $d^6\underline{L}$ [16].

We tried to fit the experimental Mössbauer spectra of $\mathrm{Fe_3PO_7}$ assuming an alternative conical spin structure proposed in a previous neutron-diffraction study of polycrystalline samples $\mathrm{Fe_3PO_7}$ [2]. This structure is characterized by the conical axis ($\boldsymbol{n}$) directed along the crystal $\boldsymbol{a}$ axis ($\boldsymbol{n} \parallel \boldsymbol{a}$) and the opening angle $\alpha \approx 70^\circ$ (see Fig. S2 of the Supplemental Material [27]), which produces a good fit to the neutron-diffraction pattern [2]. Figure S1 of the Supplemental Material [27] shows the fitted spectra (recorded at $T = 15$ K) for different values of the anisotropic hyperfine field $H_{\mathrm{an}}(= A_{\mathrm{an}}S)$ and the opening angle (α) (a detailed description is given in the Supplemental Material [27]). As we can see from this figure, despite the number of variable parameters, this model does not allow us to account for the shape of the experimental spectra. Therefore, the presented Mössbauer data allow us to give some preference to the helicoidal phase-modulated spin structure. A similar choice between the above two models is difficult to discern from the neutron powder diffraction data [2].

IV. CONCLUSIONS

We have carried out detailed ^{57}Fe Mössbauer measurements on polycrystalline samples of $\mathrm{Fe_3PO_7}$ that demonstrated the effectiveness of the suggested approach to an analysis of the complex hyperfine magnetic structure of the spectra measured over a wide temperature range. The results presented above not only confirm several features of the helicoidal magnetic structure in $\mathrm{Fe_3PO_7}$, but they also allow the helical plane direction, which cannot be determined from neutron powder diffraction data, to be refined. It has been shown that a good fitting of the experimental spectra can be achieved assuming that the electric hyperfine interactions are modulated when the Fe^{3+} spin rotates with respect to the EFG axis, and with the emergence of spatial anisotropy of the hyperfine field H_{hf} at ^{57}Fe nuclei. The large anharmonicity parameter, $m \approx 0.94$, of the spiral spin structure resulting from easy-axis anisotropy in the plane of the iron spin rotation can be related to the needlelike domains within the hexagonal (ab) plane. The Mössbauer spectra of $\mathrm{Fe_3PO_7}$ cannot be described using an alternative conical spin structure proposed in previous neutron-diffraction studies. Analysis of the temperature dependence $H_{\mathrm{hf}}(T)$ with the Bean-Rodbell model leads to the structural factor $\zeta \approx 0.53$, which suggests that the magnetic phase transition is second-order in nature but with strong coupling magnetic ordering to the lattice deformation. The lower value of the saturated magnetic field $H_{\mathrm{hf}}(0) \approx 462$ kOe is mainly related to the magnetic surrounding of Fe^{3+} ions via the supertransferred hyperfine field and the large negative contribution $H_{\mathrm{cov}} \approx -168$ kOe arising from the Fe^{3+}-$O^{2-} \rightarrow Fe^{2+}$-$O^{-}(\underline{L})$ charge transfer. The DFT calculations yield reliable charge distribution to which the EFG is so sensitive. It was shown that, in addition to the lattice contribution $\boldsymbol{V}^{\mathrm{lat}}$, very large weight has an electronic contribution $\boldsymbol{V}^{\mathrm{el}}$ arising from the asymmetric distribution of the *p* core and 3*d* valence electrons. From the calculated occupation number, the fluctuation of Δn_d is more pronounced than that of Δn_p, indicating a stronger anisotropic spatial distribution of Fe^{3+} 3*d* electrons. It was found that 3*d* electrons move from d_{x2-y2} and d_{xy} orbitals to d_{xz}, d_{yz}, and d_{zz} orbitals, which correlates with the local symmetry of the distorted trigonal bipyramid ($\mathrm{FeO_5}$) clusters. Such electronic redistribution in the low-symmetry crystal field may give the small anisotropic contribution $\sim(\tilde{\boldsymbol{A}}^{\mathrm{orb}} + \tilde{\boldsymbol{A}}^{\mathrm{dip}}) \cdot \boldsymbol{S}$ in the hyperfine field $\boldsymbol{H}_{\mathrm{hf}}$ at ^{57}Fe nuclei. However, we have shown that the main contribution to the observed anisotropy of $\boldsymbol{H}_{\mathrm{hf}}$ is due to the anisotropy of the dipole field $\tilde{\boldsymbol{A}}^{\mathrm{D}}$ induced by the neighboring iron ions.

[1] C. Cipriani, M. Mellini, G. Pratesi, and C. Viti, Eur. J. Mineral. **9**, 1101 (1997).
[2] K. A. Ross, M. M. Bordelon, G. Terho, and J. R. Neilson, Phys. Rev. B **92**, 134419 (2015).
[3] A. Modaressi, A. Courtois, R. Gerardin, B. Malaman, and C. Gleitzer, J. Solid State Chem. **47**, 245 (1983).
[4] G. Gavoille, C. Gleitzer, and G. J. Long, Rev. Chim. Miner. **24**, 42 (1987).

[5] M. E. Matsnev and V. S. Rusakov, in *Mössbauer Spectroscopy in Materials Science 2012*, edited by J. Tuček and M. Miglierini, AIP Conf. Proc. (AIP, New York, 2012), Vol. 1489, p. 178; in *Mössbauer Spectroscopy in Materials Science 2012*, edited by J. Tuček and M. Miglierini, AIP Conf. Proc. (AIP, New York, 2014), Vol. 1622, p. 40.
[6] P. Blaha, J. Phys.: Conf. Ser. **217**, 012009 (2010).
[7] F. Neese, Comput. Mol. Sci. **2**, 73 (2012).
[8] A. D. Becke, J. Chem. Phys. **98**, 5648 (1993); C. Lee, W. Yang, and R. G. Parr, Phys. Rev. B **37**, 785 (1988).
[9] F. Weigend and R. Ahlrichs, Phys. Chem. Chem. Phys. **7**, 3297 (2005).
[10] F. Menil, J. Phys. Chem. Solids **46**, 763 (1985).
[11] P. Gütlich, E. Bill, and A. X. Trautwein, *Mössbauer Spectroscopy and Transition Metal Chemistry, Fundamentals and Applications* (Springer Verlag, Berlin Heidelberg, 2011).
[12] K. Schwarz, C. Ambrosch-Draxl, and P. Blaha, Phys. Rev. B **42**, 2051 (1990).
[13] R. S. Mulliken, J. Chem. Phys. **23**, 1833 (1955).
[14] A. Palewicz, T. Szumiata, R. Przeniosło, I. Sosnowska, and I. Margiolaki, Solid State Commun. **140**, 359 (2006).
[15] V. Rusakov, V. Pokatilov, A. Sigov, M. Matsnev, and T. Gubaidulina, J. Mat. Sci. Eng. **B4**, 302 (2014).
[16] A. Sobolev, V. Rusakov, A. Moskvin, A. Gapochka, A. Belik, I. Glazkova, A. Akulenko, G. Demazeau, and I. Presniakov, J. Phys.: Condens. Matter **29**, 275803 (2017).
[17] D. Colson, A. Forget, and P. Bonville, J. Magn. Magn. Mater. **378**, 529 (2015).
[18] M. Eibschütz and M. E. Lines, Phys. Rev. B **25**, 4256 (1982).
[19] A. V. Zalesskiĭ, A. K. Zvezdin, A. A. Frolov, and A. A. Bush, JETP Lett. **71**, 465 (2000).
[20] C. P. Bean and D. S. Rodbell, Phys. Rev. **126**, 104 (1962).
[21] A. Taroni, S. T. Bramwell, and P. C. W. Holdsworth, J. Phys.: Condens. Matter **20**, 275233 (2008).
[22] G. A. Sawatzky and F. van der Woude, J. Phys. (Paris) Colloq. **35**, C6-47 (1974).
[23] A. S. Moskvin, N. S. Ovanesyan, and V. A. Trukhtanov, Hyperfine Interact. **5**, 13 (1977).
[24] C. Boekema, P. C. Jonker, G. Filoti, F. van der Woude, and G. A. Sawatzky, Hyperfine Interact. **7**, 45 (1979).
[25] A. S. Moskvin, N. S. Ovanesyan, and V. A. Trukhtanov, Hyperfine Interact. **3**, 429 (1977).
[26] R. E. Watson and A. J. Freeman, Phys. Rev. **123**, 2027 (1961).
[27] See Supplemental Material at http://link.aps.org/supplemental/10.1103/PhysRevB.97.104415 for additional details of the Mössbauer simulation using conical spin structure, and additional details and results from DFT calculations.